J|A|C|S

A R T I C L E S

Allosteric Inhibition of Protein−DNA Complexes by Polyamide−Intercalator Conjugates

Eric J. Fechter and Peter B. Dervan*

Contribution from the Division of Chemistry and Chemical Engineering, California Institute of Technology, Pasadena, California 91125

Received February 21, 2003; E-mail: dervan@caltech.edu

Abstract: The sequence-specific inhibition of essential protein−DNA contacts in the promoter of a gene is a central issue for the regulation of gene expression by chemical methods. Hairpin polyamides have been shown to inhibit protein−DNA complexes in some but not all cases. For example, polyamides co-occupy the same DNA sequence in the minor groove in the presence of major-groove binding bZip proteins. Four hairpin polyamide−acridine conjugates were synthesized and shown to bind the minor groove of DNA with high affinity in a sequence-specific manner. The polyamide−acridine conjugates were shown to unwind DNA ($\phi = 14-15°$), evidence for intercalation by the acridine moiety. Importantly, the polyamide−intercalator conjugates, which combine sequence-specific groove binding with proximal local unwinding, inhibit major-groove DNA binding by the GCN4 bZip protein. This class of DNA binding molecules creates a sequence-specific allosteric change in DNA structure and has the potential to be a general inhibitor of transcription factor binding independent of the specific protein−DNA structure.

Introduction

Controlling gene expression with DNA binding small molecules is a challenge at the interface of chemistry and biology.[1] Toward this goal, a crucial step is to inhibit essential transcription factors from binding specific DNA elements in the promoter of a gene.[2] During the past decade, the X-ray and NMR structures of a large number of protein−DNA complexes have been reported.[3−7] There are distinct families of protein motifs which are recurring themes in DNA complexes, such as zinc fingers,[4] bZip,[5] and winged helix−turn−helix.[6] In a formal sense, there are at least two mechanisms by which synthetic ligands might compete with specific protein−DNA binding: direct steric interference or an allosteric alteration of DNA structure or some combination of both. One strategy is to consider each family of protein−DNA complexes as a unique target and, from a consideration of the complex structure, arrive at a protein-specific strategy for inhibition by a polyamide binding in the minor groove.[8−16] In the simplest case, a minor-

groove binding protein would be inhibited by a minor-groove binding polyamide for reasons of steric blockade.[8−11] A major-groove/minor-groove binding protein also would be inhibited by judicious placement of the polyamide near crucial protein minor-groove contacts.[9] A major-groove protein that distorts DNA from a B-form helix, either by bending or alteration of groove width, might not be compatible with a minor-groove polyamide that prefers B-form. Indeed, recent studies have documented that pyrrole−imidazole polyamides, which bind sequence specifically in the minor groove of DNA, are able to block several different classes of eukaryotic transcription factors (TFs) from binding their cognate DNA sites.[8−16] For example, the general transcription factor TATA box-binding protein (TBP) and the lymphoid enhancer factor (LEF-1) can be inhibited by steric interference with minor-groove contacts as well as "locking" the DNA into a B-type conformation upon polyamide binding.[9] Allosteric inhibition may also extend to a class of major-groove binding TFs that recognize sites containing narrow

(1) (a) Dervan, P. B. *Bioorg. Med. Chem.* **2001**, *9*, 2215−2235. (b) Gottesfeld, J. M.; Turner, J. M.; Dervan, P. B. *Gene Expression* **2000**, *9*, 77−91. (c) Nielsen, P. E. *Curr. Med. Chem.* **2001**, *8*, 545−550. (d) Giovannangeli, C.; Hélène, C. *Curr. Opin. Mol. Ther.* **2000**, *2*, 288−296.
(2) (a) Pandolfi, P. P. *Oncogene* **2001**, *20*, 3116−3127. (b) Darnell, J. E. *Nat. Rev.-Cancer* **2002**, *2*, 740−749.
(3) (a) Kim, J. L.; Nikolov, D. B.; Burley, S. K. *Nature* **1993**, *365*, 520−527. (b) Kim, Y. C.; Geiger, J. H.; Hahn, S.; Sigler, P. B. *Nature* **1993**, *365*, 512−520.
(4) Pavletich, N. P.; Pabo, C. O. *Science* **1991**, *252*, 809−817.
(5) (a) Ellenberger, T. E.; Brandl, C. J.; Struhl, K.; Harrison, S. C. *Cell* **1992**, *71*, 1223−1237. (b) Keller, W.; Konig, P.; Richmond, T. J. *J. Mol. Biol.* **1995**, *254*, 657−667.
(6) Garvie, C. W.; Hagman, J.; Wolberger, C. *Mol. Cell.* **2001**, *8*, 1267−1276.
(7) (a) Love, J. J.; Li, X. A.; Case, D. A.; Giese, K.; Grosschedl, R.; Wright, P. E. *Nature* **1995**, *376*, 791−795. (b) Lang, D.; Stamminger, T. *Nucleic Acids Res.* **1994**, *22*, 3331−3338. (c) Chen, F. E.; Huang, D. B.; Chen, Y. Q.; Ghosh, G. *Nature* **1998**, *391*, 410−413. (d) Ferredamare, A. R.; Prendergast, G. C.; Ziff, E. B.; Burley, S. K. *Nature* **1993**, *363*, 38−45.

(8) Neely, L.; Trauger, J. W.; Baird, E. E.; Dervan, P. B.; Gottesfeld, J. M. *J. Mol. Biol.* **1997**, *274*, 439−445.
(9) Dickinson, L. A.; Gulizia, R. J.; Trauger, J. W.; Baird, E. E.; Mosier, D. E.; Gottesfeld, J. M.; Dervan, P. B. *Proc. Natl. Acad. Sci., U.S.A.* **1998**, *95*, 12890−12895.
(10) McBryant, S. J.; Baird, E. E.; Trauger, J. W.; Dervan, P. B.; Gottesfeld, J. M. *J. Mol. Biol.* **1999**, *286*, 973−981.
(11) Ehley, J. A.; Melander, C.; Herman, D.; Baird, E. E.; Ferguson, H. A.; Goodrich, J. A.; Dervan, P. B.; Gottesfeld, J. M. *Mol. Cell. Biol.* **2002**, *22*, 1723−1733.
(12) Dickinson, L. A.; Trauger, J. W.; Baird, E. E.; Ghazal, P.; Dervan, P. B.; Gottesfeld, J. M. *Biochemistry* **1999**, *38*, 10801−10807.
(13) Lenzmeier, B. A.; Baird, E. E.; Dervan, P. B.; Nyborg, J. K. *J. Mol. Biol.* **1999**, *291*, 731−744.
(14) Wurtz, N. R.; Pomerantz, J. L.; Baltimore, D.; Dervan, P. B. *Biochemistry* **2002**, *41*, 7604−7609.
(15) Dickinson, L. A.; Trauger, J. W.; Baird, E. E.; Dervan, P. B.; Graves, B. J.; Gottesfeld, J. M. *J. Biol. Chem.* **1999**, *274*, 12765−12773.
(16) Winston, R. L.; Ehley, J. A.; Baird, E. E.; Dervan, P. B.; Gottesfeld, J. M. *Biochemistry* **2000**, *39*, 9092−9098.
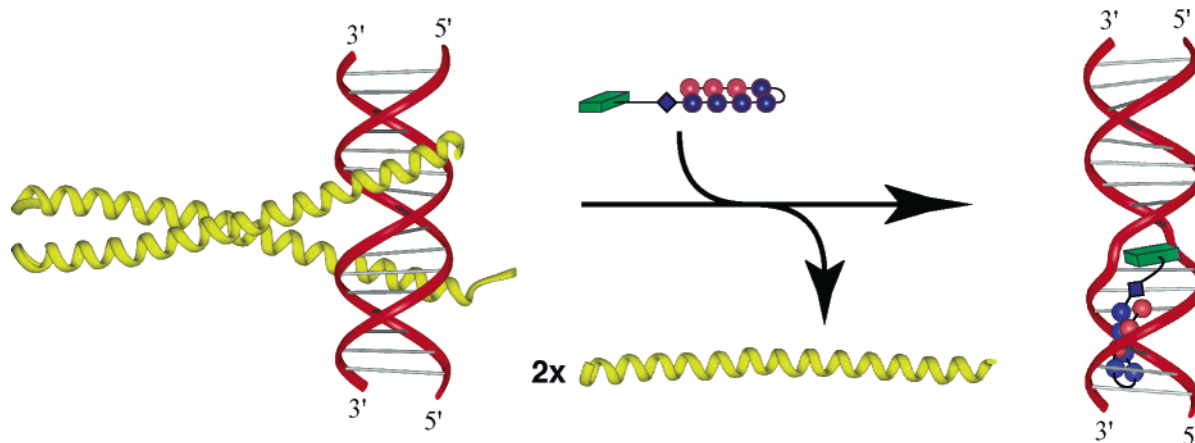
Figure 1. Model for allosteric inhibition of a protein−DNA complex by a polyamide−intercalator conjugate. The GCN4 homodimer (yellow) is displaced by the intercalating moiety (green) of the polyamide conjugate. Blue and red spheres represent pyrrole and imidazole amino acids, respectively. The blue diamond represents β-alanine.

minor grooves, such the NF-κB heterodimer, by widening the minor groove upon polyamide binding.[14] Proteins recognizing specific sequences in the major groove with additional contacts to phosphates outside the groove, such as the winged−helix−turn−helix TF (Ets-1)[6] and the basic helix−loop−helix (bHLH),[7d] provide another means of inhibition through phosphate interference by polyamides.[15,16] However, some essential DNA binding proteins remain resistant to inhibition by polyamide binding. For example, minor-groove binding polyamides can co-occupy binding sites of major-groove binding proteins such as the bZip class.[17] Presumably, polyamide contacts are confined to the minor groove[18] and the protein is confined to the major groove[5] with negligible DNA structural changes induced by either ligand.[18] One successful bZip-specific strategy was the design of polyamides containing an Arg-Pro-Arg positive patch which competes with protein side chains for electrostatic phosphate contacts on the DNA backbone.[19,20] Nonetheless, Arg-Pro-Arg-polyamides are limited to targeting phosphate contacts and are not likely to significantly disrupt the DNA topology of TF binding sites. The importance of major-groove contacts in TF-DNA complexes provides an impetus for the development of a general class of polyamides that can selectively inhibit any DNA protein complex.

There are many TF binding sites in the promoters of key genes where there is no structural information regarding the protein−DNA complex. This underlines the need to find a general solution for polyamide design that will inhibit the binding of any TF regardless of knowledge of the protein−DNA structure. One possible solution is sequence-specific, bifunctional molecule that distorts the DNA helix upon binding. The sequence-specific alteration of DNA structure would disrupt essential protein−DNA contacts. One such class of molecules
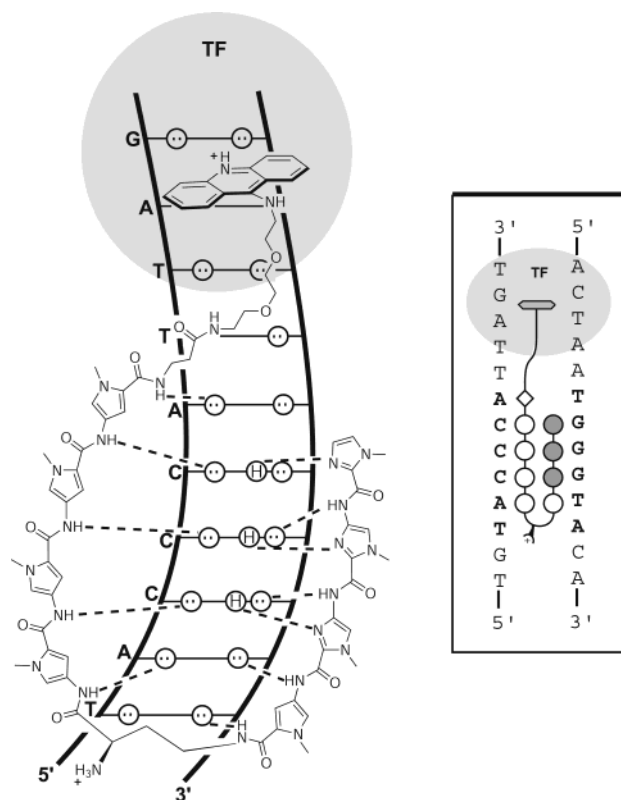
(17) (a) Oakley, M. G.; Mrksich, M.; Dervan, P. B. *Biochemistry* **1992**, *31*, 10969−10975. (b) Oakley, M. G.; Dervan, P. B. *Science* **1990**, *248*, 847−850.
(18) (a) Kielkopf, C. L.; White, S.; Szewczyk, J. W.; Turner, J. M.; Baird, E. E.; Dervan, P. B.; Rees, D. C. *Science* **1998**, *282*, 111−115. (b) Kielkopf, C. L.; Baird, E. E.; Dervan, P. B.; Rees, D. C. *Nat. Struct. Biol.* **1998**, *5*, 104−109.
(19) (a) Bremer, R. E.; Baird, E. E.; Dervan, P. B. *Chem. Biol.* **1998**, *5*, 119−133. (b) Bremer, R. E.; Wurtz, N. R.; Szewczyk, J. W.; Dervan, P. B. *Bioorg. Med. Chem.* **2001**, *9*, 2093-2103.
(20) See also: (a) White, C. M.; Satz, A. L.; Bruice, T. C.; Beerman, T. A. *Proc. Natl. Acad. Sci.* **2001**, *98*, 10590−10595. (b) He, G. X.; Browne, K. A.; Groppe, J. C.; Blasko, A.; Mei, H. Y.; Bruice, T. C. *J. Am. Chem. Soc.* **1993**, *115*, 7061−7071. (c) Browne, K. A.; He, G. X.; Bruice, T. C. *J. Am. Chem. Soc.* **1993**, *115*, 7072−7079.

Figure 2. (Left) Hydrogen-bonding model of the eight ring hairpin polyamide conjugate ImImImPy-(R)$^{H_2N\gamma}$-PyPyPyPy-β-Do-Acr bound to the minor groove of 5′-TACCCAT-3′. Circles with dots represent lone pairs of N3 of purines and O2 of pyrimidines. Circles containing an H represent the N2 hydrogens of guanine. Putative hydrogen bonds are illustrated by dotted lines. The large shaded circle represents the GCN4 transcription factor (TF). (Right) Ball and stick model of the polyamide−conjugate binding its target site (bold) adjacent to the binding of the protein GCN4. Filled circles denote imidazole, open circles represent pyrrole, and the diamond represents β-alanine. The shaded bar depicts the acridine intercalator.

would be a minor-groove binding−intercalator hybrid with the specificity of a polyamide for DNA recognition and the alteration of DNA structure by intercalator-induced local unwinding and helix extension. The insertion of flat intercalators between adjacent base pairs of the double helix causes a 3.4 Å extension and a 10−26° unwinding, depending on the aromatic moiety.[21] This localized distortion is usually confined to within

1: ImImImPy-(R)$^{\text{H}_2\text{N}}$γ-PyPyPyPy-β-Do-Acr

2: ImImImPy-(R)$^{\text{H}_2\text{N}}$γ-PyPyPyPy-β-To-Acr

3: ImImImPy-(R)$^{\text{H}_2\text{N}}$γ-PyPyPyPy-β-Do-DACA

4: ImImImPy-(R)$^{\text{H}_2\text{N}}$γ-PyPyPyPy-β-To-DACA

5a: ImImImPy-(R)$^{\text{H}_2\text{N}}$γ-PyPyPyPy-β-Do

5b: ImImImPy-(R)$^{\text{H}_2\text{N}}$γ-PyPyPyPy-β-To

5c: ImImImPy-(R)$^{\text{H}_2\text{N}}$γ-PyPyPyPy-β-Dp
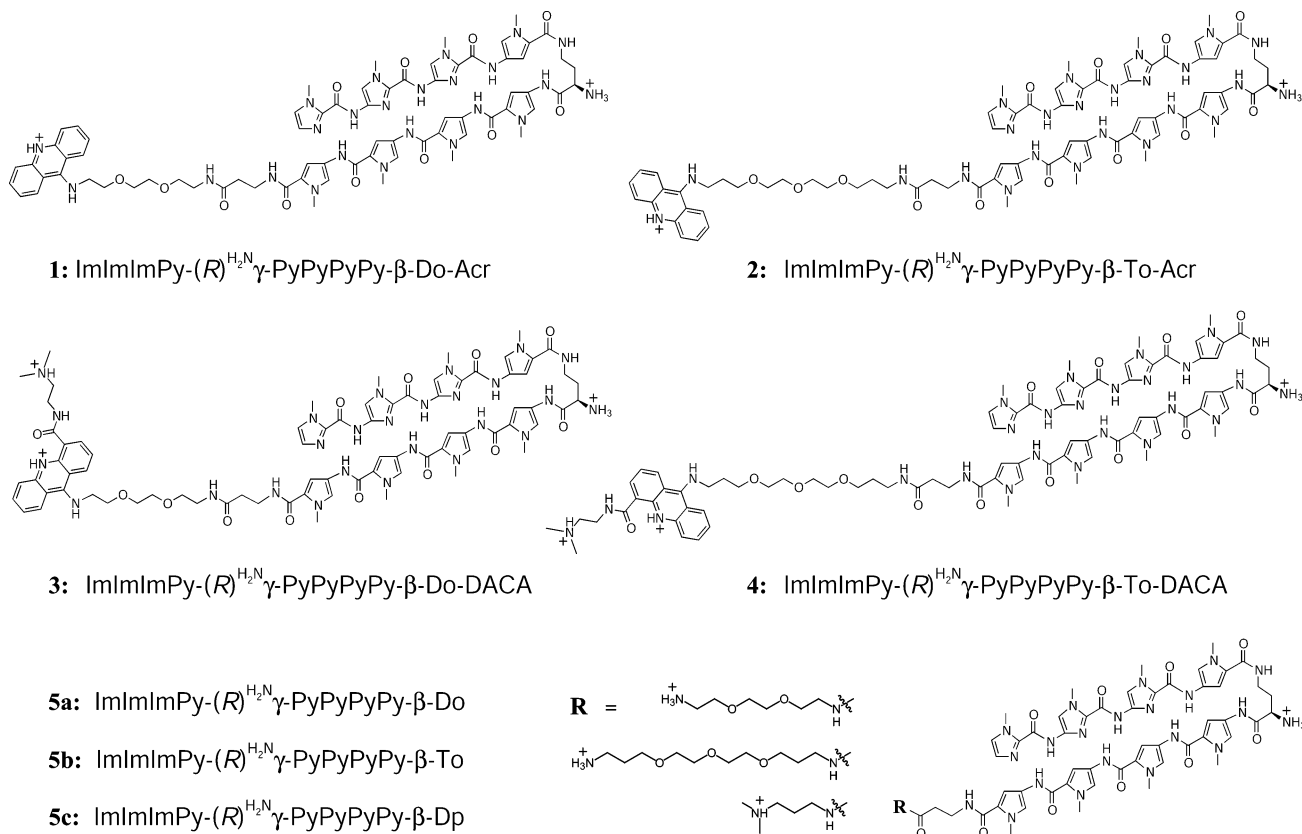
R =

Figure 3. Structures of the hairpin polyamide−acridine conjugates. Do represents 2,2′-(ethylenedioxy)bis(ethylamine), and To represents 4,7,10-trioxa-1,13-tridecanediamine.

a few base pairs of the intercalation site and shows little dependence on DNA sequence.[21,22]

A key design issue is whether the groove binding hairpin polyamide can retain its capacity for sequence discrimination when covalently linked to an intercalator (Figures 1 and 2). An effective design of sequence-specific DNA intercalation by polyamide−intercalator conjugates requires the polyamide to associate with high affinity and selectivity with simultaneous intercalation at a proximal DNA site. The covalent linkage between the two moieties should freely accommodate both modes of binding. The selected intercalator must provide sufficient DNA unwinding to disrupt TF contacts without disrupting the array of hydrogen bonds necessary for high polyamide−DNA association and specificity.

We report here the synthesis of four polyamide−acridine conjugates **1**−**4** and their abilities to selectively inhibit the major-groove binding bZip transcription factor GCN4. Polyamides were covalently linked to a 9-chloroacridine or *N*-(2-(dimethylamino)ethyl)-9-chloroacridine-4-carboxamide with one of two poly(ethylene glycol) (PEG) linkers (Figure 3). The class of acridine intercalators was chosen for its relatively modest degree of unwinding (15−17°),[22,23] preference for intercalation via the minor groove, and favorable cellular uptake properties which could be important in cell culture applications.[23−25]

Within this class, *N*-(2-(dimethylamino)ethyl)acridine-4-carbox-amide (DACA) and its derivatives are classified as "threading" intercalators given that the cationic carboxamide side chain, *peri* to the heterocyclic nitrogen, has been shown to sterically block regions of the major groove, providing greater potential for TF complex inhibition.[25,26] The DNA binding affinity and specificity of each conjugate, as well as analogues lacking the acridine unit, were evaluated using quantitative DNase I footprinting. Binding site size was measured using methidiumpropyl−EDTA (MPE) footprinting. Intercalation unwinding angles were determined using closed-circular DNA (ccDNA) methods developed by Crothers and Zeman.[27] An electrophoretic mobility shift assay (EMSA) using the carboxy-terminal 60 amino acids (222−281) of the GCN4 leucine zipper dimerization domain was used to evaluate inhibition of bZIP protein−DNA binding.

Results

Synthesis of Polyamide−Acridine Conjugates 1−4. Eight-ring hairpin polyamide conjugates containing the sequence ImImImPy-(R)$^{\text{NHFmoc}}$γ-PyPyPyPy-β-Pam-resin were synthesized in a stepwise manner on Boc-β-alanine Pam resin using established Boc-chemistry protocols.[28] The Fmoc-protected diaminobutyric acid (DABA) "turn" monomer was then depro-

(21) (a) Lerman, L. S. *J. Mol. Biol.* **1961**, *3*, 18−30. (b) Denny, W. A. *Anti-Cancer Drug Des.* **1989**, *4*, 241−263. (c) Baguley, B. C. *Anti-Cancer Drug Des.* **1991**, *6*, 1−35. (d) Wang, A. H. J. *Curr. Opin. Struct. Biol.* **1992**, *2*, 361−368.
(22) Gale, E. F.; Cundliffe, E.; Reynolds, P. E.; Richmond, M. H.; Waring, M. J. *The Molecular Basis of Antibiotic Action*, 2nd ed.; John Wiley & Sons: New York, 1981.
(23) Sakore, T. D.; Reddy, B. S.; Sobell, H. M. *J. Mol. Biol.* **1979**, *135*, 763−785.
(24) Crenshaw, J. M.; Graves, D. E.; Denny, W. A. *Biochemistry* **1995**, *34*, 13682−13687.
(25) Todd, A. K.; Adams, A.; Thorpe, J. H.; Denny, W. A.; Wakelin, L. P. G.; Cardin, C. J. *J. Med. Chem.* **1999**, *42*, 536−540.
(26) (a) Atwell, G. J.; Cain, B. F.; Baguley, B. C.; Finlay, G. J.; Denny, W. A. *J. Med. Chem.* **1984**, *27*, 1481−1485. (b) Denny, W. A.; Atwell, G. J.; Rewcastle, G. W.; Baguley, B. C. *J. Med. Chem.* **1987**, *30*, 658−663.
(27) (a) Zeman, S. M.; Depew, K. M.; Danishefsky, S. J.; Crothers, D. M. *Proc. Natl. Acad. Sci.* **1998**, *95*, 4327−4332. (b) Zeman, S. M.; Crothers, D. M. *Methods Enzymol.* **2001**, *340*, 51−68.
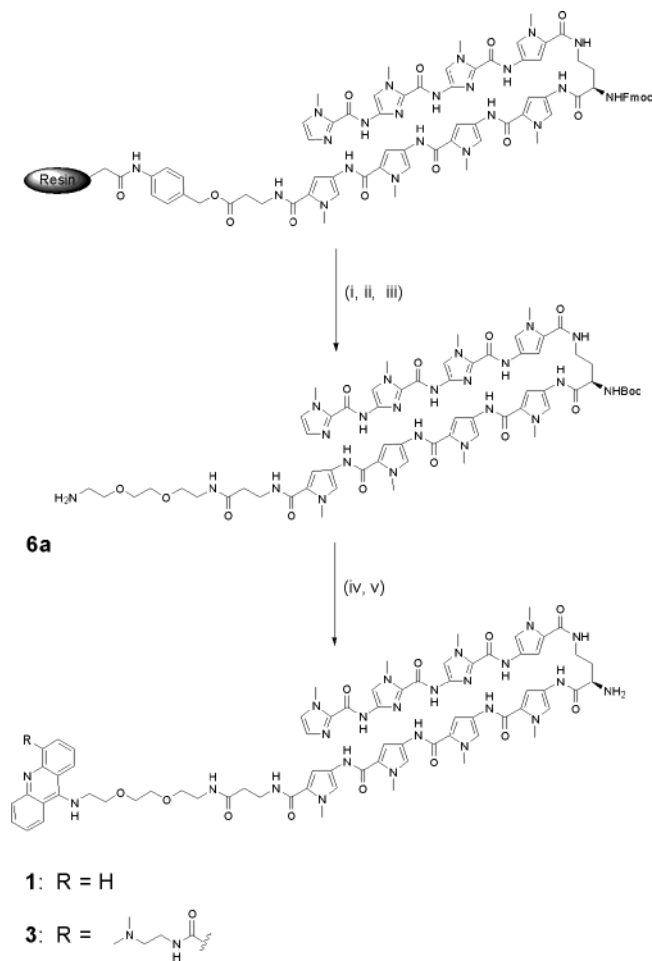(28) Baird, E. E.; Dervan, P. B. *J. Am. Chem. Soc.* **1996**, *118*, 6141−6146.

Figure 4. Synthetic scheme for polyamide–acridine conjugates: (i) 4:1 piperidine–DMF, 25 °C (30 min); (ii) Boc$_2$O, DIEA, NMP, 55 °C (30 min); (iii) 2,2′-(ethylenedioxy)-bis(ethylamine), 55 °C (18 h); (iv) 9-chloroacridine or *N*-(2-(dimethylamino)ethyl)-9-chloroacridine-4-carboxamide, phenol, DIEA, 100 °C (1 h); (v) 80% TFA/DCM, 0.4 M PhSH, 25 °C (15 min).

tected by treatment with piperidine, followed by reprotection with Boc$_2$O prior to polyamide aminolytic cleavage using one of two diamine linking agents (Figure 4). After reverse-phase HPLC purification, the polyamide primary amine was allowed to react with 9-chloroacridine derivatives in phenol at elevated temperature in the presence of diisopropylethylamine (DIEA). The crude material was then deprotected with trifluoroacetic acid (TFA), and the desired conjugate was purified by preparatory reverse phase HPLC.

Binding Energetics and Sequence Specificity. Quantitative DNase I footprint titrations were performed on a 5′-^{32}P-labeled PCR-amplified fragment of pEF10 (Figure 5) to determine the equilibrium association constants (K_a) of polyamides **1–4** (Table 1). The amplified fragment contains two polyamide match sites 5′-TAGGGTA-3′ (**I** and **III**) and two polyamide mismatch sites 5′-TAGGCTA-3′ (**II** and **IV**). Each site contains either an upstream AT-rich (**I** and **II**) or GC-rich (**III** and **IV**) flanking sequence to evaluate the significance of the intercalation site composition on conjugate binding. The control compound **5c** contains a C-terminal *N,N*-dimethylaminopropylamine (Dp) monomer and was used as a baseline for comparing binding energetics ($K_a = 1.1 \times 10^{10}$ M^{-1} and 8.7×10^9 M^{-1} for sites **I** and **III**, respectively). Replacing the Dp residue with PEG-linked primary amines (polyamides **5a** and **5b**) results in a

decreased binding affinity at both match sites ($K_a = 3.8 \times 10^9$ M^{-1} and 4.5×10^9 M^{-1} for site **I**, respectively, and $K_a = 3.3 \times 10^9$ M^{-1} and 3.5×10^9 M^{-1} for site **III**, respectively). However, the addition of either acridine intercalator to either PEG linker (**1–4**) recovers the lost binding affinity at both match sites (example shown in Figure 6). Acridine conjugates **1** and **2**, containing both short and long PEG linkers, respectively, bound to the AT flanked match site (**I**) with the highest affinities ($K_a = 1.8 \times 10^{10}$ M^{-1} and 1.4×10^{10} M^{-1}, respectively). Each showed a slight preference (~1.5-fold) for the AT-flanked match sequence (**I**) over the GC match sequence (**III**). The specificity over mismatch sites was maintained for compound **2** and slightly decreased for the shorter linked compound **1**. The DACA-containing counterparts, conjugates **3** and **4**, showed slightly lower affinities ($K_a = 7.5 \times 10^9$ M^{-1} and 7.1×10^9 M^{-1}, respectively) for the AT-flanked match site (**I**) but a slight preference (~1.5-fold) for the GC-flanked match site (**III**) ($K_a = 9.5 \times 10^9$ M^{-1} and 1.3×10^{10} M^{-1}, respectively). The specificity over mismatch sites was again maintained for the longer linked compound **4** and slightly decreased for the shorter linked compound **3**.

Binding Site Size. Additional support for intercalative binding of conjugates **1–4** is provided by methidiumpropyl–EDTA (MPE) footprinting, wherein the binding site size can be determined at much higher resolution than by DNase I methods. MPE footprints (Figure 6b) confirm that conjugates **1–4** bind to the designed 7-bp match sites **I** and **III**. Binding to the mismatch sites **II** and **IV** is only observed at significantly higher polyamide concentrations. Protection patterns for conjugates **1–4** (Figure 6d) reveal increases in binding site size by two base pairs compared to nonconjugated controls **5a** and **5b**.

Helical Unwinding Angle Determination. To confirm intercalation and quantitatively measure the unwinding effects of the polyamide conjugates, compounds **1** and **4** were selected for helical unwinding assays using closed-circular pUC19 DNA.[27] Relaxation reactions were carried out on pUC19 preequilibrated with varying concentrations of polyamides[29] or pUC19 alone. Following topoisomerase I (Topo I) treatment and extraction of intercalated conjugate, the two-dimensional (2D) agarose gel electrophoresis of ccDNA for all reactions containing conjugates **1** and **4** resulted in a primarily negative distribution of topoisomers (Figure 7a, left). Control experiments lacking polyamide resulted in a primarily positive distribution of topoisomers (Figure 7a, right). Mathematical treatment of the difference in the most abundant topoisomers between control and polyamide–acridine conjugate reactions showed decreasing apparent unwinding angles (ϕ_{ap}) for simultaneously decreasing conjugate and plasmid concentrations (Figure 7c). The actual unwinding angles (ϕ), determined from the ordinate intercepts in Figure 7c, are 14.5° and 15.3° for conjugates **1** and **4**, respectively. Polyamide controls **5a** and **5b** lacking an acridine intercalator showed no unwinding of pUC19 (Supporting Information Figure 1).

Effects of Polyamide–Acridine Conjugates on Major-Groove Protein–DNA Complex Formation. The ability of polyamide–acridine conjugates to selectively inhibit the association of a major-groove binding protein with DNA was

---

(29) All relaxation reactions were run at a sufficiently high (and constant) binding site-to-polyamide ratio to ensure that unwinding effects were only caused by sequence-specific interactions.[27]
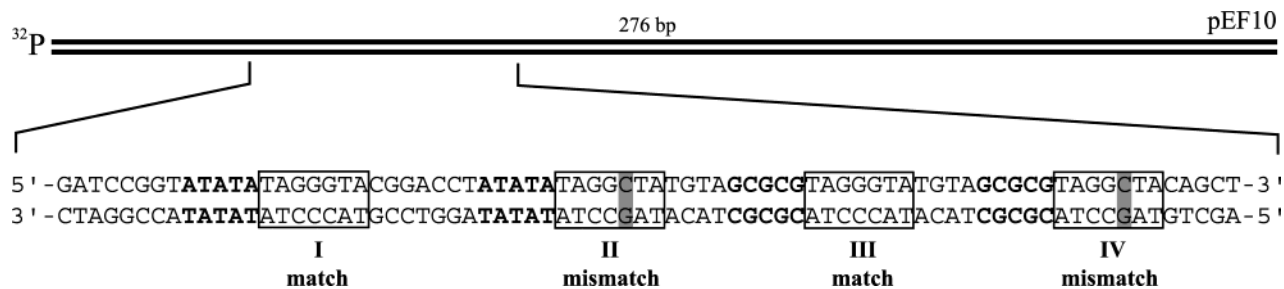
Figure 5. Sequence of the synthesized insert from the pEF10 plasmid containing two 7-bp target match sites (**I** and **III**) and two single bp mismatch sites (**II** and **IV**). Target sites are shown in boxes, and mismatch sites are shaded.

Table 1. Equilibrium Association Constants (M^{-1})^a

polyamide	site I 5′-*ATATA*TAGGG TA-3′	site II 5′-*ATATA*TAGG**C** TA-3′	site III 5′-*GCGCG*TAGGG TA-3′	site IV 5′-*GCGCG*TAGG**C** TA-3′
1	1.8 ($\pm$0.2) $\times$ 10^{10}	4.1 ($\pm$0.5) $\times$ 10^9	1.4 ($\pm$0.2) $\times$ 10^{10}	1.8 ($\pm$0.1) $\times$ 10^9
2	1.4 ($\pm$0.1) $\times$ 10^{10}	1.5 ($\pm$0.2) $\times$ 10^9	8.9 ($\pm$0.8) $\times$ 10^9	5.8 ($\pm$0.8) $\times$ 10^8
3	7.5 ($\pm$0.6) $\times$ 10^9	1.0 ($\pm$0.1) $\times$ 10^9	9.5 ($\pm$0.9) $\times$ 10^9	1.1 ($\pm$0.1) $\times$ 10^9
4	7.1 ($\pm$0.5) $\times$ 10^9	8.8 ($\pm$1.0) $\times$ 10^8	1.3 ($\pm$0.1) $\times$ 10^{10}	1.5 ($\pm$0.1) $\times$ 10^9
5a	3.8 ($\pm$0.7) $\times$ 10^9	4.2 ($\pm$0.5) $\times$ 10^8	3.3 ($\pm$0.4) $\times$ 10^9	1.4 ($\pm$0.1) $\times$ 10^8
5b	4.5 ($\pm$0.4) $\times$ 10^9	4.8 ($\pm$0.4) $\times$ 10^8	3.5 ($\pm$0.3) $\times$ 10^9	1.1 ($\pm$0.2) $\times$ 10^8
5c	1.1 ($\pm$0.1) $\times$ 10^{10}	1.1 ($\pm$0.2) $\times$ 10^9	8.7 ($\pm$1.3) $\times$ 10^9	4.2 ($\pm$0.6) $\times$ 10^8

^{a} The reported association constants are the average values obtained from three DNase I footprint titration experiments. The standard deviation for each data set is indicated in parentheses. The flanking intercalation sites are indicated in italics, and the mismatch sites are shown in bold. Assays were performed at 22 °C at pH 7.0 in the presence of 10 mM Tris·HCl, 10 mM KCl, 10 mM MgCl$_2$, and 5 mM CaCl$_2$.

tested using the basic DNA binding domain of the GCN4 (222−281) homodimer.[30] Inhibition was first determined by performing an EMSA of the ^{32}P radiolabeled 33-bp DNA duplex, ARE−41, which contains a GCN4-binding site (5′-CTGACTAAT-3′)[17] and a single flanking polyamide binding site (5′-TGGGTA-3′) oriented such that the acridine moieties of the bound polyamides **1**−**4** were directed toward the TF binding site. All four polyamide conjugates significantly inhibited GCN4−DNA complex formation. Representative gels show shifted bands from complexed to free DNA for compounds **1**−**3** as the conjugate concentrations were increased from 1nM to 1μM in the presence of 200 nM concentration of GCN4 (see Supporting Information Figure 2) (Figure 8a, lanes 3−15). The mobility of the DNA duplex was unaffected by the addition of polyamide alone (Figure 8a, lane 16). Quantitation of shifted lanes by comparison to control lane 2 (containing only DNA and GCN4) provides percent inhibition curves (Figure 8b). Conjugates **1** and **3** were the most effective of the series (65−80% complex inhibition) with IC$_{50}$ values of ~10 nM. Conjugate **2** showed 60−65% inhibition, while compound **4** attained slightly less than 60% complex inhibition. Control compounds **5a** and **5b** corresponding to polyamides containing PEG diamine linkers, but lacking acridine or DACA, were unable to inhibit GCN4 binding (Supporting Information Figure 3).

Inhibition studies were then carried out using the 40-bp duplex ARE−53. This duplex contains the same GCN4 and polyamide binding site as ARE−41, with an additional flanking polyamide binding site proximal to the GCN4 binding domain (Figure 9a). The effects of two binding conjugates increased the TF inhibition of all compounds to near quantitative amounts[31] while reducing the IC$_{50}$ values to sub-nanomolar concentrations. Conjugates tested on the analogous ARE−53−1M duplex (Figure 9b),

containing internal single base-pair mismatches (as with sites **II** and **IV** on pEF10) at both polyamide binding sites, resulted in more than 20% decreased inhibition and increased IC$_{50}$ values (>10 nM, Figure 9c).

Discussion

There are several examples of DNA-binding natural products, such as actinomycin D and triostin A, which use bimodal cooperative intercalation/groove binding for molecular recognition of DNA.[32,33] Early design efforts toward artificial mimics of these natural products combined modules of intercalators, such as acridine or phenoxazone, and groove binders derived from netropsin and distamycin.[34] Intercalators and minor-groove binding polyamides affect DNA conformation in very different ways. Intercalators unwind and extend the helix by 3.4 Å, while crescent-shaped minor-groove binders disrupt the DNA minimally, maintaining a relatively undistorted shape of the B-form helix.[18] DNA structural distortion remote from the site of intercalation and extending over four base pairs could possibly disrupt essential minor-groove contacts by the polyamide ring pairs. Therefore, the choice of linker length and flexibility is crucial for optimum cooperative binding of both modules. Indeed, one would prefer that the two binding domains function independently, i.e., the polyamide defines the target sequence with little sequence preference superimposed by the intercalator, and the intercalator unwinds locally with little constraint from the adjacent polyamide.

Our results show that polyamide−acridine conjugates are capable of maintaining the binding affinity and sequence specificity when compared to the parent hairpins. The loss of

(30) The 60 amino acid sequence (222−281) of GCN4 contains the 'leucine zipper' dimerization domain and the 'basic region' responsible for DNA binding.

(31) The effects of polyamide−acridine conjugates binding only to the upstream site showed similar GCN4 inhibition values as ARE−41.

(32) Muller, W.; Crothers, D. M. *J. Mol Biol.* **1968**, *35*, 251−290.

(33) (a) Waring, M. J.; Wakelin, L. P. G. *Nature* **1974**, *252*, 653−657. (b) Wang, A. H. J.; Ughetto, G.; Quigley, G. J.; Hakoshima, T.; van der Marel, G. A.; van Boom, J. H.; Rich, A. *Science* **1984**, *225*, 1115−1121.

(34) (a) Dervan, P. B. *Science* **1986**, *232*, 464−471. (b) Bailly, C.; Henichart, J. P. *Bioconjugate Chem.* **1991**, *2*, 379−393. (c) Carrasco, C.; Helissey, P.; Haroun, M.; Baldeyrou, B.; Lansiaux, A.; Colson, P.; Houssier, C.; Giorgi-Renault, S.; Bailly, C. *ChemBio.Chem.* **2003**, *4*, 50−61.
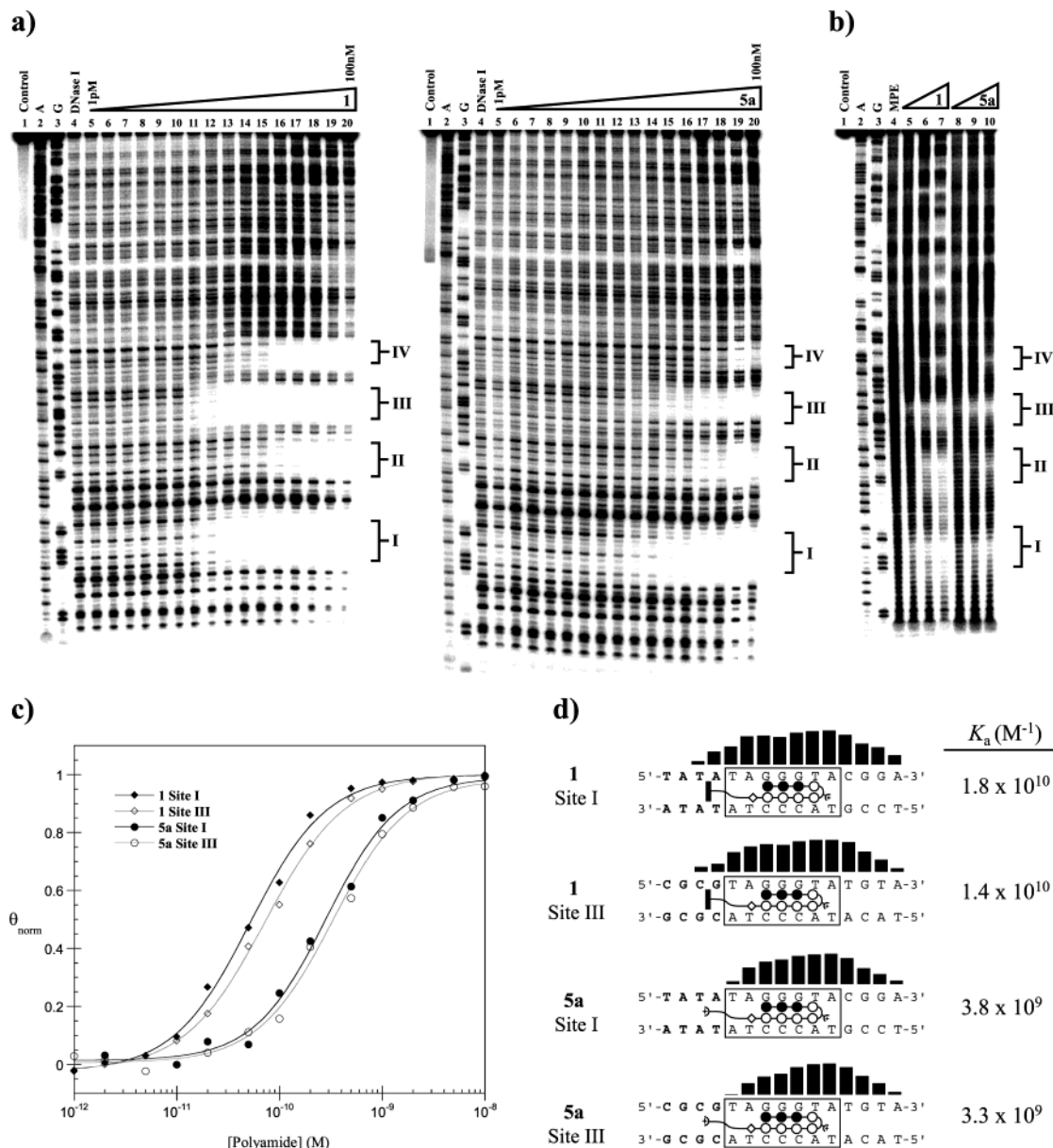
Figure 6. (a) Quantitative DNase I footprint titration experiments with ImImImPy-(R)$^{H_2N\gamma}$-PyPyPyPy-β-Do-Acr (**1**) and ImImImPy-(R)$^{H_2N\gamma}$-PyPyPyPy-β-Do (**5a**) on the PCR-amplified 5′-^{32}P-labeled 276-bp fragment of pEF10. **I**, **II**, **III**, and **IV** correspond to the sites indicated in Figure 5: Lane 1, intact DNA; lane 2, A reaction; lane 3, G reaction; lane 4, DNase I standard; lanes 5, 6, 7, 8, 9, 10, 11, 12, 13, 14, 15, 16, 17, 18, 19, and 20, 1 pM, 2 pM, 5 pM, 10 pM, 20 pM, 50 pM, 100 pM, 200 pM, 500 pM, 1 nM, 2 nM, 5 nM, 10 nM, 20 nM, 50 nM, 100 nM polyamide, respectively. All reactions contain 15 kcpm amplified fragment, 10 mM Tris·HCl (pH 7.0), 10 mM KCl, 10 mM MgCl$_2$, and 5 mM CaCl$_2$. Data were obtained for the binding sites indicated to the right of the gel. (b) MPE·Fe^{II} footprinting of **1** and **5a**: Lane 1, intact DNA; lane 2, A reaction; lane 3, G reaction; lane 4, MPE·Fe^{II} standard; lanes 5, 6, and 7, 200 pM, 2 nM, and 20 nM **1**; lanes 8, 9, and 10, 200 pM, 2 nM, and 20 nM **5a**. (c) Binding isotherms at match sites for **1** and **5a**. θ_{norm} points were obtained using storage phosphor autoradiography and processed by standard methods. Each data point shows the average value obtained from three footprinting experiments. The solid curves are best-fit Langmuir binding titration isotherms obtained from nonlinear least squares algorithm. (d) MPE·Fe^{II} protection patterns at 2 nM concentration for each match site. Bar heights are proportional to the relative protection from cleavage at each band. K_a values of the corresponding match sites are shown to the right.

affinity by replacement of the C-terminal Dp monomer with a PEG linker (**5a** and **5b**) is consistent with studies in our group. The recovery of affinity upon the addition of an acridine intercalator to the PEG linker (without changing the net cationic charge in the cases of **1** and **2**) suggests that the acridine moiety participates in DNA binding. The binding affinity of polyamide–acridine conjugate **1** is $K_a = 1.8 \times 10^{10}$ M^{-1}, a 5-fold increase over the parent polyamide **5a**, $K_a = 3.8 \times 10^9$ M^{-1}. From previous work, the affinity of 9-aminoacridine can be estimated to be $K_a \approx 7 \times 10^4$ M^{-1}.[24] Since the energetic gain for the linked acridine is modest, a factor of 5-fold rather than

10^5, i.e., $K_a^{conjugate} < (K_a^{polyamide}) \times (K_a^{acridine})$, we conclude there is a negative cooperative association of the combined ligands to DNA. Additionally, the modest preference for GC flanking sequences by **3** and **4** is consistent with the previously reported binding affinities of DACA and its derivatives.[26] As with unconjugated DACA, compounds **3** and **4** may allow the carboxamide side chain to reside in the major groove and become stabilized by a specific hydrogen bond between the $-NMe_2H^+$ group to the N7 of guanine, leading to the modest GC binding preference.[25] The increased affinity from the side chain association may be slightly offset by an unfavorable steric
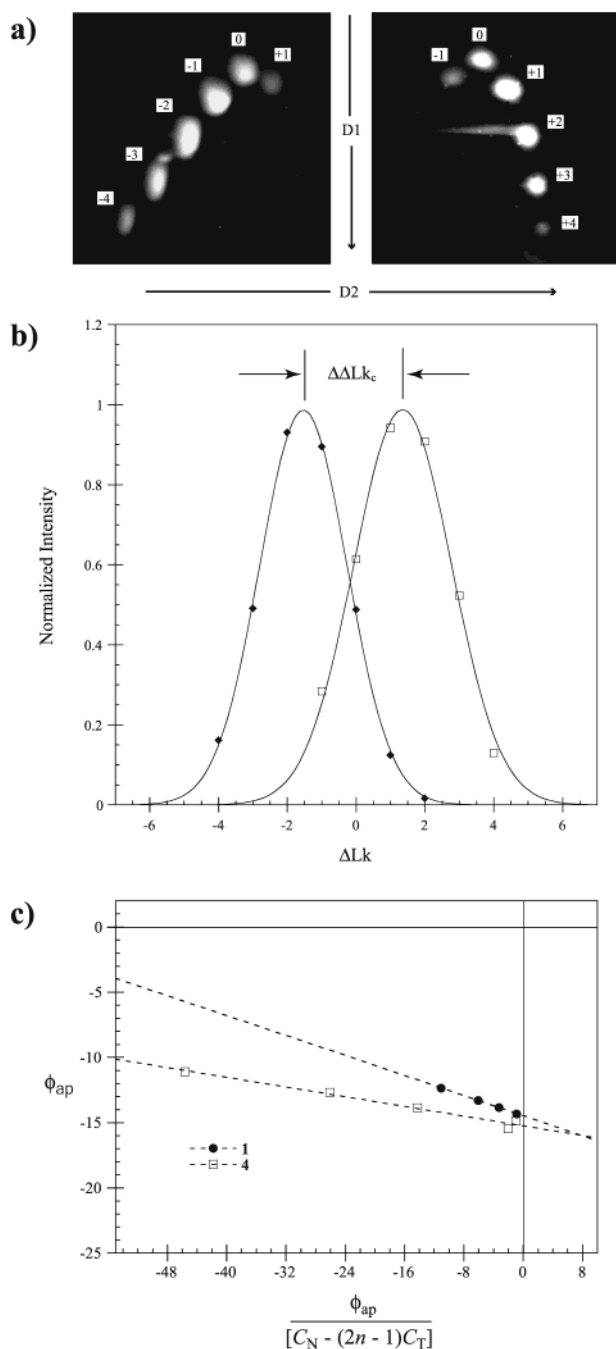
a)

b)

c)

Figure 7. (a) Images of topoisomer bands from reactions containing and lacking polyamide–acridine conjugate **1**, (top left and top right, respectively). The directions of electrophoresis and ΔLk values are shown. (b) The corresponding Boltzman distributions (extracted from normalized band intensities) are shown below their gels. (c) Binding isotherms for polyamide–acridine conjugates **1** (●) and **4** (□). Each data point was calculated from one set of distributions (as in part a). The ordinate intercept yields the canonical unwinding angle (φ) per polyamide–acridine conjugate.

interaction of the PEG linker with the exocyclic NH_2 in the minor groove of guanine-rich sequences. This steric effect should exist for the compounds lacking the carboxamide side chain **1** and **2** and may account for the slight preference for AT flanking sequences.

The sequence specificity of the conjugates with longer linkers **2** and **4** was maintained, while that of the conjugates with shorter linkers **1** and **3** showed a slight decrease. This result suggests that the trioxa-diamine linker (To) was sufficiently long to
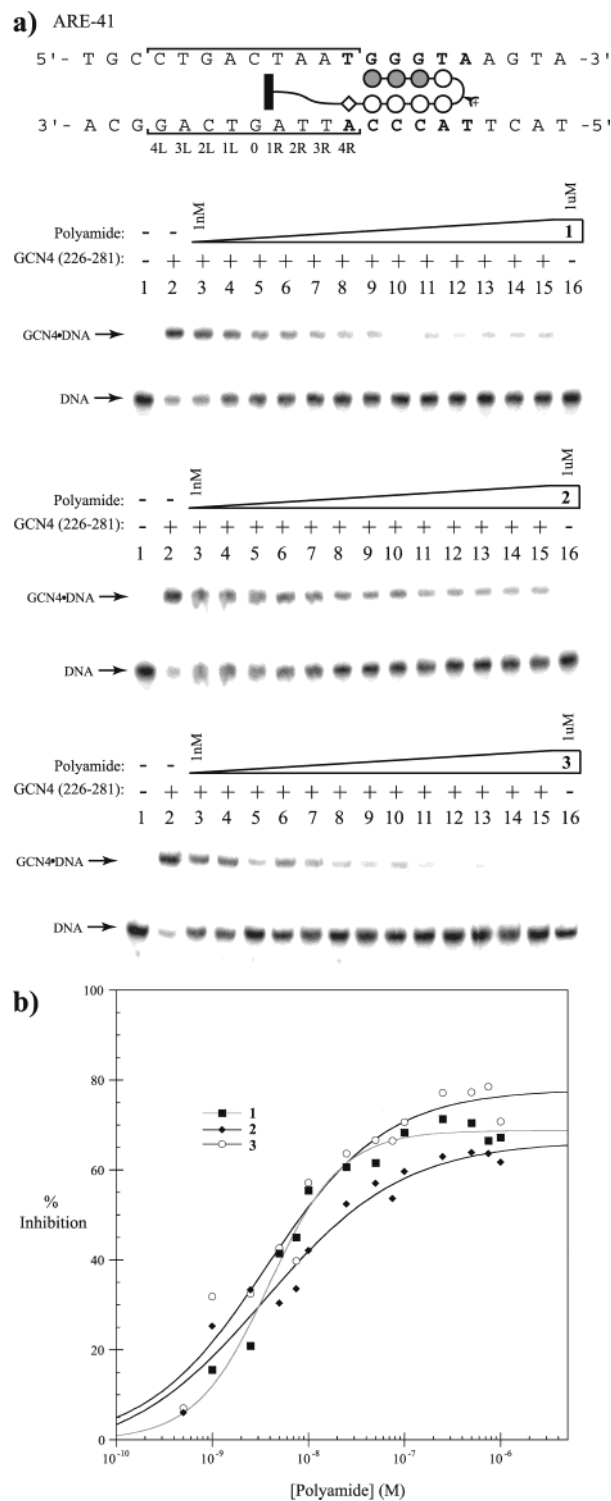
a) ARE-41

b)

Figure 8. (a) Representative GCN4 (222−281) electrophoretic mobility shift assay results for conjugates **1**, **2**, and **3** with ARE−41. The pseudopalindromic GCN4 binding site is shown in brackets and the base pair assignments shown below the duplex. The polyamide binding site is shown as bold text. Polyamide symbols are as in Figure 2. The storage phosphor autoradiograms of **1**−**3** are shown below the duplex with visibly shifted bands in the presence of increasing concentrations of polyamide−conjugate. Upper band, GCN4 (222−281)−DNA complex; lower band, free DNA; lane 1, DNA only; lane 2, DNA incubated with 100 nM GCN4 (222−281); lanes 3, 4, 5, 6, 7, 8, 9, 10, 11, 12, 13, 14, and 15 are 100 nM GCN4 (222−281) and 1 nM, 2.5 nM, 5 nM, 7.5 nM, 10 nM, 25 nM, 50 nM, 75 nM, 100 nM, 250 nM, 500 nM, 750 nM, and 1 μM **1**, **2**, or **3**, respectively; lane 16, DNA with 1 μM polyamide. (b) Inhibition curves for polyamide conjugate effects on formation of GCN4 (222−281)−DNA complex.
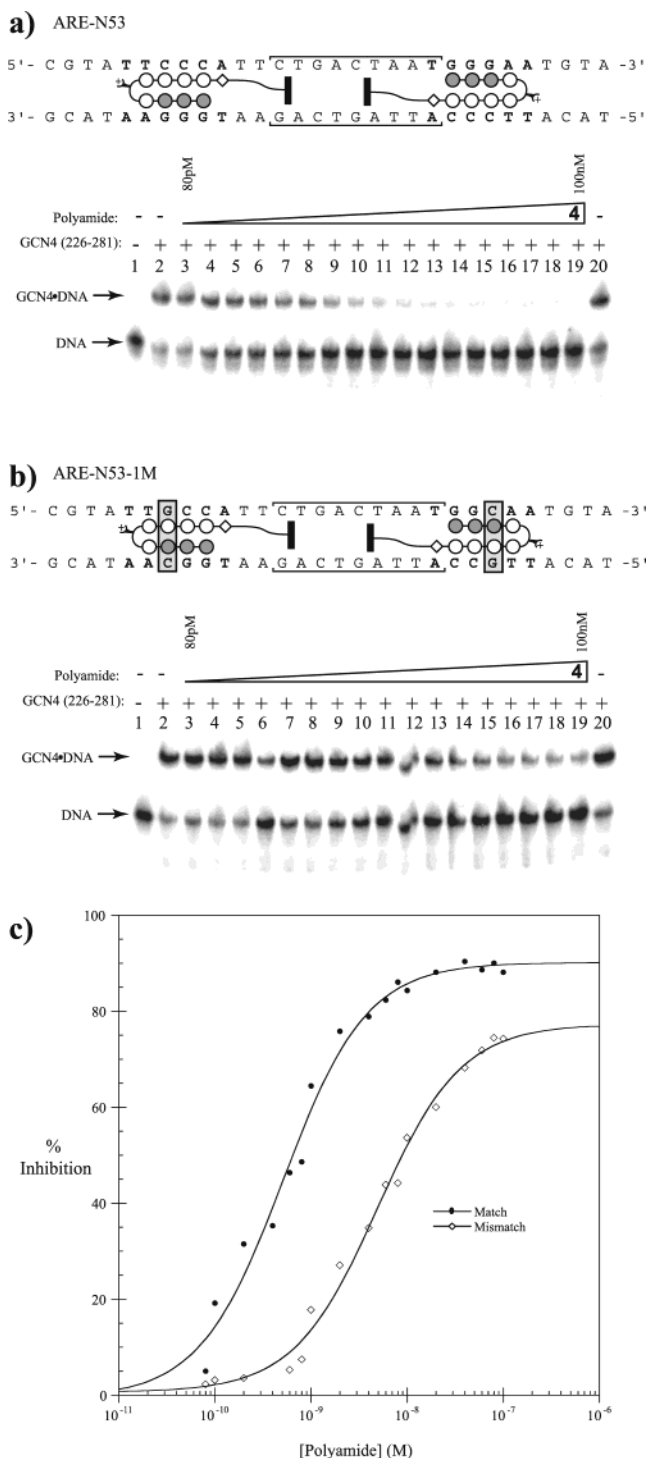
Figure 9. Representative GCN4 (222–281) electrophoretic mobility shift assay results for conjugate **4** with (a) duplex ARE-N53 containing two polyamide match sites and (b) duplex ARE-N53−1M containing two single base-pair mismatch sites. Symbols for polyamides are indicated in Figure 2. Lane 1, DNA only; lanes 2 and 20, DNA incubated with 100 nM GCN4 (222–281); lanes 3, 4, 5, 6, 7, 8, 9, 10, 11, 12, 13, 14, 15, 16, 17, 18, and 19 are 100 nM GCN4 (222–281) and 80 pM, 100 pM, 200 pM, 400 pM, 600 pM, 800 pM, 1 nM, 2 nM, 4 nM, 6 nM, 8 nM, 10 nM, 20 nM, 40 nM, 60 nM, 80 nM, and 100 nM **4**. (c) Inhibition curves for polyamide−conjugate effects on formation of GCN4 (222–281)−DNA complex with two flanking polyamide match sites (solid circles) and two flanking polyamide mismatch sites (open diamonds).

permit mutual minor-groove and intercalative binding without interrupting the hydrogen bonds essential for high polyamide association and specificity. The shorter dioxa-diamine linker

(Do) may direct the intercalator nearer the polyamide, preventing optimal mutual binding and dislocating key recognition elements.

MPE footprinting reveals a binding-site size increase for conjugates **1**−**4** by two base pairs. The saturation intercalation conditions of MPE footprinting result in at least every other potential methidium intercalation site unoccupied (neighbor exclusion). The intercalation of conjugates **1**−**4** would therefore prevent intercalation of methidium at the site adjacent to the polyamide N-terminus (albeit not the case if strictly groove binding) and in turn prevent strand cleavage at this site. The nearest possible location for strand cleavage using the intercalative model of **1**−**4** would be two base pairs past the N-terminus of the control polyamide (Figure 6b).

The unwinding assay provides evidence that the conjugates simultaneously intercalate while binding to the minor groove. Since parent hairpin polyamides had no effect on DNA unwinding (Supporting Information Figure 1), the total unwinding is attributed to the tethered intercalating moiety. The helical unwinding angle (ϕ) of the polyamide−DACA conjugate **4** was consistent with reported values for the unconjugated intercalator, indicating that conjugation using the trioxa-diamine linker (To) does not compromise the propensity of intercalation. However, conjugate **1** showed an average ϕ of ∼2.5° less than the reported value for 9-aminoacridine.[22] The attenuated ϕ of conjugate **1** suggests that the slightly shorter linker (Do) may not be optimal for maximum occupancy of the intercalator moiety within DNA, in agreement with the DNase I footprinting data. The polyamide may disrupt the orientation of the intercalator within the base-pair stack resulting in the slight decrease in ϕ. We cannot rule out that the difference in unwinding properties of the acridine intercalator may be explained by the changes in chromophore electronics such as enhanced electrostatic associations upon conjugation.

Gel mobility shift experiments on conjugates **1**−**4** show that **1** and **3** effectively inhibit major-groove binding of GCN4. CPK modeling suggests that the intercalation site with these compounds extends between three and four base pairs past the β-alanine unit of the polyamide. On the basis of published GCN4 basic region−DNA crystal structures,[5] it is an interesting exercise to speculate on the local topological perturbations caused by site-specific intercalation (Figure 10). Between base-pair sites 0 and 1R the conjugate may locally disrupt two phosphate interactions (Arg243 and Thr236), one hydrophobic interaction (Ala239) and one hydrogen bond (Arg243) of right-half site GCN4 monomer. Additionally, a phosphate interaction (Arg240) and hydrogen bond (Arg243) at the center of binding (position 0) from the left-half site monomer may be altered. This arginine contact is considered crucial for anchoring the protein to the center of the binding site. Besides the immediate contacts affected, more distal allosteric disruptions, such as widening of the major groove and increased relative twist of the two ends of the duplex by intercalation, most likely contribute to the decreased affinity of GCN4. The slightly lower GCN4 inhibition by conjugates containing longer linkers **2** and **4** may be accounted for by intercalation at other sites and failing to unwind the duplex at the specified contacts.

The duplex ARE−53, containing a second polyamide binding site, provided increased inhibition of GCN4. The proposed intercalation site for the added conjugate with dioxa-diamine
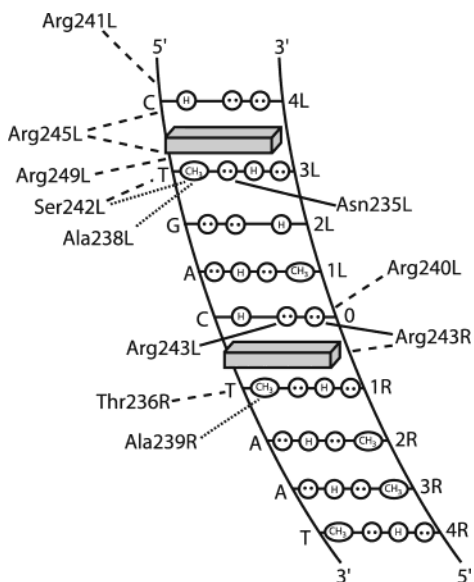
Figure 10. Predicted major-groove contacts of the GCN4 dimer directly affected by intercalation of **3** or **4** in ARE-N53. Intercalating chromophores are shown as shaded blocks. Protein side-chain contacts made by the left-half site monomer end with L, while contacts made by the right-half site monomer end with R. The CG base pair at position 0 represents the center of the DNA pseudodyad. Solid lines represent hydrogen bonds, dashed lines represent phosphate contacts, and dotted lines represent van der Waals interactions. Circles with two dots depict the lone pairs of the N7 of purines, the O4 of thymine, and the O6 of guanine. Circles containing an H represent the N6 and N4 hydrogens of the exocyclic amines of adenine and cytosine, respectively. The C5 methyl group of thymine is shown as a circle with CH$_3$ inside.

linkers **1** or **3** falls between the 3L and 4L base pairs. This site houses a large concentration of critical contacts, including four phosphate interactions (Arg241, Arg245, Arg249, and Ser242), two hydrophobic interaction (Ser242 and Ala238), and one hydrogen bond (Asn235), lying deep within the major groove. Overall, the combined effect of both intercalation sites could be the direct disruption of nearly one-half of the identified contacts of the GCN4 complex. The longer linked trioxa-diamine conjugates **2** and **4** showed equal inhibition, indicating that the precise location of critical GCN4 contacts relative to intercalation is not as crucial when two conjugate binding sites are present. The duplex containing one core mismatch for each binding site (ARE−53−1M) demonstrates inhibition selectivity with an IC$_{50}$ value of approximately 1 order of magnitude higher than its corresponding match sequence in agreement with mismatch affinities from DNase I footprinting results.

Conclusion. Hairpin polyamide−acridine conjugates have been shown to selectively inhibit a protein binding exclusively to the major groove. The conjugates intercalate and bind to the minor groove without sacrificing affinity or specificity. By delivering an intercalating moiety to a specified region of DNA from a tethered polyamide, this class of molecules should be a general method for targeting a broad array of protein−DNA complexes of interest.

Experimental Section

Materials. 9-Chloroacridine was purchased from Pfaltz & Bauer, Inc. *N*-(2-(Dimethylamino)ethyl)-9-chloroacridine-4-carboxamide was synthesized according to published procedures.[26a] Restriction endonucleases were purchased from New England Biolabs and used as noted in the manufacturer's protocol. Sequenase (version 2.0) was obtained from Boeringher-Mannheim. [α-^{32}P]-Thymidine-5′-triphosphate (≥3000

Ci/mmol) and [α-^{32}P]-deoxyadenosine-5′-triphosphate (≥6000 Ci/ mmol) were purchased from DuPont/NEN. [γ-^{32}P]-Adenosine-5′-triphosphate (≥6000 Ci/mmol) was obtained from ICN. Purified pUC19 DNA for unwinding angle determination was isolated from transformed JM109 *Escherichia coli* using the Qiagen protocol. EDTA, dithiothreitol (DTT), ultrapure agarose, and calf thymus Topo I were purchased from GIBCO/BRL. Micron 50 microconcentrators were purchased from Amicon. ProbeQuant G-50. Micro Columns were purchased from Amersham Pharmacia Biotech, Inc. GCN4 (222−281) prepared by solid-phase synthesis was generously provided by Martha G. Oakley. Water (18 MΩ) was obtained from a Millipore MilliQ water purification system, and all buffers were 0.2 μm filtered. Reagent-grade chemicals were used as received unless otherwise stated.

UV spectra were measured on a Beckman Coulter DU7400 diode array spectrophotometer. Matrix-assisted, laser desorption/ionization time-of-flight mass spectrometry (MALDI-TOF) was performed using an Applied Biosystems Voyager DE-Pro. HPLC analysis was performed on a Beckman Gold system using a RAININ C$_{18}$, Microsorb MV, 5 μm, 300 × 4.6 mm reversed-phase column in 0.1% (v/v) TFA with acetonitrile as eluent and a flow rate of 1.0 mL/min. Preparatory reversed-phase HPLC was performed on a Beckman HPLC using a Waters DeltaPak 25 × 100 mm, 100 μm C$_{18}$ column equipped with a guard, 0.1% (wt/v) TFA, 0.25% acetonitrile/min.

ImImImPy-(R)$^{H_2N\gamma}$-PyPyPyPy-β-Do-Acr (1). Compound **6a** (1 μmol aliquot) was added to 100 μL of phenol and dissolved by heating to 100 °C. To this solution was added 9-chloroacridine (0.5 M, 3 μL) in DMF, followed by 10 μL of DIEA, and the reaction was allowed to proceed at 100 °C for 1 h. The mixture was then cooled to 50 °C and diluted with 0.1% (wt/v) TFA (100 μL). The mixture was then further cooled to room temperature and treated with 1 mL of 80% TFA/DCM, 0.4 M PhSH. After 30 min the mixture was diluted with 0.1% (wt/v) TFA and the resulting solution purified by reversed-phase HPLC. Lyophilization provided ImImImPy-(R)$^{H_2N\gamma}$-PyPyPyPy-β-Do-Acr (**1**) as a yellow powder (0.50 mg, 41% recovery). MALDI-TOF-MS (monoisotopic) calcd for C$_{71}$H$_{81}$N$_{24}$O$_{12}$ (M+H): 1461.7. Found: 1461.7.

ImImImPy-(R)$^{H_2N\gamma}$-PyPyPyPy-β-To-Acr (2). Synthesized as described for **1** starting from 1 μmol of **6b** (0.41 mg, 35% recovery). MALDI-TOF-MS (monoisotopic) calcd for C$_{71}$H$_{81}$N$_{24}$O$_{12}$ (M+H): 1533.7. Found: 1533.7.

ImImImPy-(R)$^{H_2N\gamma}$-PyPyPyPy-β-Do-DACA (3). Synthesized as described for **1** using *N*-(2-(dimethylamino)ethyl)-9-chloroacridine-4-carboxamide (0.5 M, 3 μL) followed by the addition of 20 μL of DIEA (0.37 mg, 11% recovery). MALDI-TOF-MS (monoisotopic) calcd for C$_{76}$H$_{91}$N$_{26}$O$_{13}$ (M+H): 1575.7. Found: 1575.9.

ImImImPy-(R)$^{H_2N\gamma}$-PyPyPyPy-β-To-DACA (4). Synthesized as described for **2** using *N*-(2-(dimethylamino)ethyl)-9-chloroacridine-4-carboxamide (0.5M, 3 μL) in DMF, followed by the addition of 20 μL of DIEA (0.45 mg, 14% recovery). MALDI-TOF-MS (monoisotopic) calcd for C$_{80}$H$_{99}$N$_{26}$O$_{14}$ (M+H): 1647.8. Found: 1647.9.

ImImImPy-(R)$^{H_2N\gamma}$-PyPyPyPy-β-Do (5a). A sample of ImImImPy-(R)$^{NHFmoc}\gamma$-PyPyPyPy-β-Pam-resin (100 mg, 0.356 mmol/g) was suspended in 2,2′-(ethylenedioxy)bis(ethylamine) and heated at 55 °C for 12 h. The reaction mixture was filtered to remove resin, 0.1% (wt/ v) TFA added (6 mL), and the resulting solution purified by reversed-phase HPLC. ImImImPy-(R)$^{H_2N}\gamma$-PyPyPyPy-β-Do (**5a**) was recovered upon lyophilization of the appropriate fractions as a yellow powder (12 mg, 24% recovery). MALDI-TOF-MS (monoisotopic) calcd for C$_{67}$H$_{90}$N$_{23}$O$_{15}$ (M+H): 1284.6. Found: 1284.9.

ImImImPy-(R)$^{H_2N\gamma}$-PyPyPyPy-β-To (5b). Synthesized as described for **5a** using 4,7,10-trioxa-1,13-tridecanediamine (2 mL) for polyamide cleavage from resin (9 mg, 18% recovery). MALDI-TOF-MS (monoisotopic) calcd for C$_{67}$H$_{90}$N$_{23}$O$_{15}$ (M+H): 1356.6. Found: 1356.8.

ImImImPy-(R)$^{H_2N\gamma}$-PyPyPyPy-β-Dp (5c). Synthesized as described for **5a** using neat *N,N*′-(dimethylamino)propylamine (2 mL) for polyamide cleavage from resin (22 mg, 46% recovery). MALDI-

TOF-MS (monoisotopic) calcd for $C_{57}H_{72}N_{23}O_{10}$ (M+H): 1238.6. Found: 1238.6.

ImImImPy-(R)^{NHBoc}cγ-PyPyPyPy-β-Do (6a). ImImImPy-(R)^{NHFmoc}γ-PyPyPyPy-β-Pam-resin was generated from Boc-β-alanine Pam resin (1 g, 0.59 mmol/g) using previously described Boc-protected monomers and methods.[28] A sample of the above polyamide on dried resin (200 mg, 0.356 mmol/g) was suspended in 4 mL of 4:1 piperidine−DMF and agitated (22 °C, 30 min). The resultant ImImImPy-(R)^{H_2N}γ-PyPyPyPy-β-Pam-resin was washed sequentially with DCM and DMF. The resin was then suspended in 4 mL of NMP to which was added 500 mg of Boc₂O followed by 1 mL of DIEA, and the mixture was agitated (55 °C, 30 min). The resultant ImImImPy-(R)^{NHBoc}γ-PyPyPyPy-β-Pam-resin was washed sequentially with DMF, DCM, MeOH, and ethyl ether, and the amine−resin was dried in vacuo. A sample of resin was then treated with neat 2,2′-(ethylenedioxy)bis(ethylamine) (2 mL) and heated (55 °C) with periodic agitation for 16 h. The reaction mixture was filtered to remove resin, 0.1% (wt/v) TFA added (6 mL), and the resulting solution purified by reversed-phase HPLC. ImImImPy-(R)^{NHBoc}γ-PyPyPyPy-β-Do (6a) was recovered upon lyophilization of the appropriate fractions as an off white powder (24 mg, 23% recovery). MALDI-TOF-MS (monoisotopic) calcd for $C_{63}H_{82}N_{23}O_{14}$ (M+H): 1384.6. Found: 1385.0.

ImImImPy-(R)^{NHBoc}γ-PyPyPyPy-β-To (6b). Synthesized as described for 6a using neat 4,7,10-trioxa-1,13-tridecanediamine (2 mL) for polyamide cleavage from resin (32 mg, 31% recovery). MALDI-TOF-MS (monoisotopic) calcd for $C_{67}H_{90}N_{23}O_{15}$ (M+H): 1456.7. Found: 1457.3.

Construction of Plasmid DNA. The plasmid **pEF10** was constructed by insertion of the following hybridized inserts into the *Bam*HI/*Hin*DIII polycloning sites in pUC19: 5′-GATCC GGTAT ATATA GGGTA CGGAC CTATA TATAG GCTAT GTAGC GCGTA GGG-TA TGTAG CGCGT AGGCT AC-3′ and 5′-AGCTG TAGCC TACGC GCTAC ATACC CTACG CGCTA CATAG CCTAT ATATA GGTCC GTACC CTATA TATAC CG-3′. The insert was obtained by annealing complementary *Hin*DIII restriction fragments of pUC19 using T4 DNA ligase. The ligated plasmid was then used to transform JM109 subcompetent cells (Promega). Colonies were selected for α-complementation on 25 mL Luria-Bertani agar plates containing 50 mg/mL ampicillin. Cells were harvested after overnight growth at 37 °C. Large-scale plasmid purification was performed using WizardPlus Midi Preps from Promega. The presence of the desired insert was determined by dideoxy sequencing.

Preparation of 5′-End-Labeled Fragments. Two 21 base-pair primer oligonucleotides, 5′-GAATT CGAGC TCGGT ACCCG G-3′ (forward) and 5′-TGGCA CGACA GGTTT CCCGA C-3′ (reverse) were constructed for PCR amplification. The forward primer was radiolabeled using [γ-^{32}P]-dATP and polynucleotide kinase, followed by purification using MicroSpin G-50 columns. The desired DNA segment was amplified as previously described.[35] The labeled fragment was loaded onto a 7% nondenaturing preparatory polyacrylamide gel (5% cross-link), and the desired 276 base-pair band was visualized by autoradiography and isolated. Chemical sequencing reactions were performed according to published protocols.[36,37]

Quantitative DNase I Footprint Titrations. All reactions were carried out in a volume of 400 μL according to published protocols.[35] Quantitation by storage phosphor autoradiography and determination of equilibrium association constants were as previously described.[35]

MPE·FeII Footprinting. All reactions were carried out in a volume of 400 μL according to published protocols.[35]

Gel Mobility Shift Assay. Radiolabeled synthetic duplex DNA was prepared for gel mobility shift assay by treating with Sequenase (version 2.0), [α-^{32}P]-thymidine-5′-triphosphate, and [α-^{32}P]-deoxyadenosine-5′-triphosphate for 3′-end labeling. The labeled duplex was purified using ProbeQuant G-50 Micro Columns. Polyamide was incubated with the duplex (20,000 cpm) in 40 μL reaction volumes of bisTris (10 mM, pH 7.0), NaCl (100 mM), DTT (1 mM), EDTA (1 mM), and poly(dI-dC)·poly(dI-dC) (5 μg/mL) for 16 h at 22 °C. GCN4 (222−281) was added and equilibrated for 45 min. Loading buffer (15% Ficoll, 0.025% bromophenol blue, 10 μL) was added, and 10 μL was immediately loaded onto a running 8% (29:1 acrylamide:bis-acrylamide) polyacrylamide gel (0.5 · TBE, 280 V, 0.8 mm, 13 cm). Separation of uncomplexed DNA and DNA-GCN4 (222−281) complexes was achieved within 40 min. Gels were dried in vacuo at 80 °C and then exposed to a storage phosphor screen (Molecular Dynamics).[38]

Unwinding Angle and Intrinsic Association Constant Determination. Relaxation reactions and numeric analyses were all carried out as described.[27] Minor variations to published protocols include two-dimensional gel electrophoresis carried out in 18 × 20 cm 1% agarose casting units and imaged after ethidium bromide staining with a Typhoon 8600 variable mode imager and 610-nm band-pass filter. The Boltzman distribution of adopted integer Lk values were plotted using the equation

$$I = I_M e^{[-w(\Delta Lk - \Delta Lk_c)^2]} \qquad (1)$$

where ΔLk and ΔLk_c are the measured linking difference and most abundant linking difference, respectively, I and I_M are integrated and maximum band intensity, respectively, and w is the distribution width. The apparent unwinding angle was calculated using the equation

$$\phi_{ap} = \frac{360 N_D (\Delta Lk_c - \Delta Lk^o_c)}{N_L} \qquad (2)$$

where ΔLk^o_c is the most abundant linking difference for the control reactions containing no polyamide and N_D and N_L are the number of pUC19 and polyamide conjugate molecules, respectively. The actual unwinding angle was calculated using the equation

$$\phi_{ap} = \phi - \frac{\phi_{ap}}{K_a[C_N - (2n - 1)C_T]} \qquad (3)$$

where n represents the number of binding sites covered by one conjugate (set to unity) and C_N and C_T represent the concentration of conjugate binding sites and the concentration of polyamide conjugate. The C_N value was approximated from 268 conjugate binding sites (and single base-pair mismatch sites) per ccDNA molecule for both 1 and 4. The value of C_N affects the slope in Figure 7c but does not influence the value of ϕ (ϕ is the ordinate intercept).

Supporting Information Available: Gel shift and unwinding experiments for polyamide controls lacking the acridine intercalator, and the GCN4 binding isotherm. This material is available free of charge via the Internet at http://pubs.acs.org.

JA030125E

(35) Trauger, J. W.; Dervan, P. B. *Methods Enzymol.* **2001**, *340*, 450−466.
(36) Maxam, A. M.; Gilbert, W. S. *Methods Enzymol.* **1980**, *65*, 499−560.
(37) Iverson, B. L.; Dervan, P. B. *Methods Enzymol.* **1996**, *15*, 7823−7830.

(38) Johnston, R. F.; Pickett, S. C.; Barker, D. L. *Electrophoresis* **1990**, *11*, 355−360.